10.24425/acs.2023.146276

Archives of Control Sciences
Volume 33(LXIX), 2023
No. 2, *pages* 277–298

A new two-scroll 4-D hyperchaotic system with a unique saddle point equilibrium, its bifurcation analysis, circuit design and a control application to complete synchronization

Sundarapandian VAIDYANATHAN, Irene M. MOROZ and Aceng SAMBAS

In this work, we present new results for a two-scroll 4-D hyperchaotic system with a unique saddle point equilibrium at the origin. The bifurcation and multi-stability analysis for the new hyperchaotic system are discussed in detail. As a control application, we develop a feedback control based on integral sliding mode control (ISMC) for the complete synchronization of a pair of two-scroll hyperchaotic systems developed in this work. Numerical simulations using Matlab are provided to illustrate the hyperchaotic phase portraits, bifurcation diagrams and synchronization results. Finally, as an electronic application, we simulate the new hyperchaotic system using Multisim for real-world implementations.

Key words: hyperchaos, hyperchaotic systems, bifurcation analysis, multi-stability analysis, synchronization, Multisim, circuit simulation

1. Introduction

Oscillators [1–3], memristors [4–6], circuits [7–9], encryption [10, 11], cryptosystems [12–14], and fuzzy systems [15, 16] are some popular areas where hyperchaotic systems find applications owing to the high complexity in their dynamics.

S. Vaidyanathan (corresponding author, e-mail: sundarvtu@gmail.com) is with Centre for Control Systems, Vel Tech University, 400 Feet Outer Ring Road, Avadi, Chennai-600092, Tamil Nadu, India.

I.M. Moroz (e-mail: Irene.Moroz@maths.ox.ac.uk) is with Mathematical Institute, University of Oxford, Andrew Wiles Building, ROQ, Oxford Ox2 6GG, UK.

A. Sambas (e-mail: acengsambas@unisza.edu.my) is with Faculty of Informatics and Computing, Universiti Sultan Zainal Abidin, Gong Badak, 21300, Terengganu, Malaysia, and (e-mail: acengs@umtas.ac.id), Department of Mechanical Engineering, Universitas Muhammadiyah Tasikmalaya, Tasikmalaya 46196, West Java, Indonesia.

Received 02.03.2022.

The modelling of two-scroll hyperchaotic systems with varying level of complexity is an active research work in chaos literature. In this work, we find a new two-scroll hyperchaotic system with a unique saddle point equilibrium at the origin. We detail the qualitative features of the two-scroll hyperchaotic system comprehensively using bifurcation diagrams with the help of Lyapunov characteristic exponents (LCE). Bifurcation analysis is very useful in unravelling the various dynamic features of a chaotic or hyperchaotic system [17–19]. We also consider the dynamics at infinity.

A multi-stability analysis of the two-scroll hyperchaotic system is also carried out by fixing the values of the system parameters in the hyperchaotic case but by considering two different initial data. Multi-stability is a special complex feature of chaotic and hyperchaotic systems [8, 9, 14].

Using Multisim, we build an electronic circuit of the new two-scroll hyperchaotic system and the outputs of the Multisim circuit cohesively demonstrate the matching with the Matlab outputs of the same system.

As a control application, we describe a complete synchronization design of a pair of two-scroll hyperchaotic systems with the help of integral sliding mode control (ISMC). Sliding mode control is a popular control technique with inherent advantages such as robustness, insensitivity to small parameter variations, fast convergence, etc. [20–22].

2. A new two-scroll hyperchaotic system with a unique saddle point equilibrium

In this work, we propose a new hyperchaotic system:

$$\begin{cases} \dot{y}_1 = a(y_2 - y_1) + py_2y_3\,, \\ \dot{y}_2 = by_2 - y_1y_3 + y_4\,, \\ \dot{y}_3 = y_1y_2 - cy_3\,, \\ \dot{y}_4 = -qy_2. \end{cases} \tag{1}$$

The state of the 4-D system (1) is designated $Y = (y_1, y_2, y_3, y_4)$.

Using Lyapunov exponents, it shall be shown in this work that the system (1) exhibits a hyperchaotic attractor when the system parameters assume the values

$$a = 40, \quad b = 28, \quad c = 3, \quad p = 0.4, \quad q = 2.5. \tag{2}$$

For $T = 1E5$ seconds, the Lyapunov characteristic exponents (LCE) of the 4-D system (1) were numerically estimated for $Y(0) = (0.4, 0.2, 0.4, 0.2)$ and $(a, b, c, p, q) = (40, 28, 3, 0.4, 2.5)$ to be:

$$l_1 = 3.0717, \quad l_2 = 0.0527, \quad l_3 = 0, \quad l_4 = -18.1354. \tag{3}$$

Thus, we conclude that the 4-D system (1) has dissipative hyperchaotic motion for the chosen values (2).

Figure 1 exhibits the Matlab plots of the 4-D system (1) for $Y(0) = (0.4, 0.2, 0.4, 0.2)$ and $(a, b, c, p, q) = (40, 28, 3, 0.4, 2.5)$.

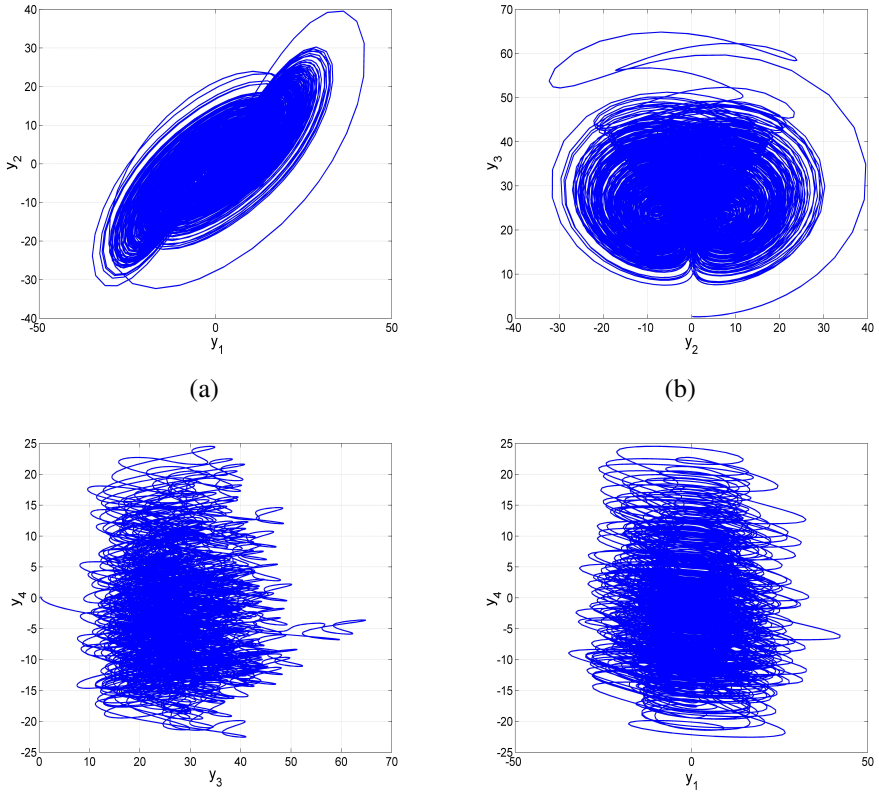

Figure 1: State orbits of the two-scroll 4-D hyperchaotic system given by (1) for $Y(0) = (0.4, 0.2, 0.4, 0.2)$ and $(a, b, c, p, q) = (40, 28, 3, 0.4, 2.5)$: (a) y_1-y_2-plane, (b) y_2-y_3-plane, (c) y_3-y_4-plane and (d) y_1-y_4-plane

To derive the fixed points of the 4-D hyperchaotic system (1), we seek the roots of the following system of equations:

$$a(y_2 - y_1) + py_2y_3 = 0 \tag{4a}$$

$$by_2 - y_1y_3 + y_4 = 0 \tag{4b}$$

$$y_1y_2 - cy_3 = 0 \tag{4c}$$

$$-qy_2 = 0 \tag{4d}$$

Since $q > 0$, (4d) implies that $y_2 = 0$.

Substituting $y_2 = 0$ into (4c), $cy_3 = 0$, and since $c > 0$, we conclude that $y_3 = 0$.

Substituting $y_2 = 0$ and $y_3 = 0$ into (4b), we find that $y_4 = 0$, and substituting $y_2 = 0$ into (4a), we see that $ay_1 = 0$.

Since $a > 0$, we conclude that $y_1 = 0$.

Hence, the unique fixed point of the 4-D system (1) is given by $B_0 = (0, 0, 0, 0)$.

The stability nature of the fixed point B_0 is found via the Jacobian or the linearized matrix J_0 of the 4-D system (1) at B_0.

Thus:

$$J_0 = \begin{bmatrix} -40 & 40 & 0 & 0 \\ 0 & 28 & 0 & 1 \\ 0 & 0 & -3 & 0 \\ 0 & -2.5 & 0 & 0 \end{bmatrix}. \tag{5}$$

The eigenvalues of J_0 are numerically estimated as follows:

$$\mu_1 = -3, \quad \mu_2 = -40, \quad \mu_3 = 0.0896, \quad \mu_4 = 27.9104. \tag{6}$$

Using the first method of Lyapunov stability theory, we deduce that B_0 is is a saddle point (and so unstable).

The new 4-D two-scroll hyperchaotic system (1) has multistability, as it exhibits two coexisting attractors for the parameters $(a, b, c, p, q) = (40, 28, 3, 0.4, 2.5)$ and two different initial data points, *viz.* $Y_0 = (0.4, 0.2, 0.4, 0.2)$ (blue orbit) and $Z_0 = (-0.6, 0.4, 0.4, -0.6)$ (red orbit).

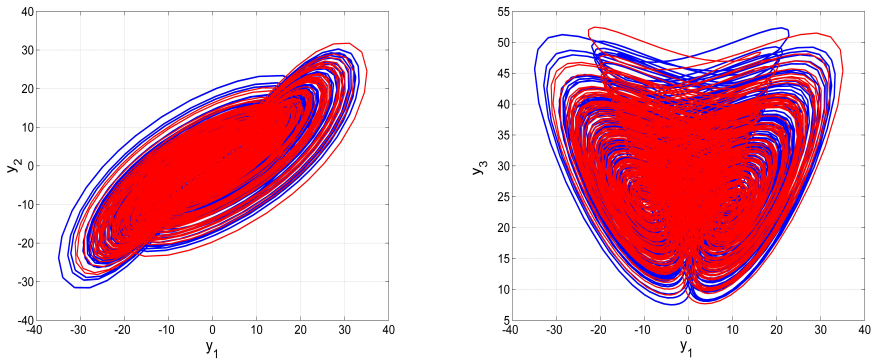

(a) (b)

Figure 2: Multistability of the 4-D two-scroll system (1): Two coexisting hyperchaotic attractors for $(a, b, c, p, q) = (40, 28, 3, 0.4, 2.5)$ and two initial phases $Y_0 = (0.4, 0.2, 0.4, 0.2)$ (blue orbit) and $Z_0 = (-0.6, 0.4, 0.4, -0.6)$ (red orbit): (a) y_1–y_2 plane and (b) y_1–y_3 plane

Figure 2 shows this coexistence of two hyperchaotic attractors for $(a, b, c, p, q) = (40, 28, 3, 0.4, 2.5)$, where the blue hyperchaotic attractor associates for the initial state $Y_0 = (0.4, 0.2, 0.4, 0.2)$ and the red hyperchaotic attractor for the initial state $Z_0 = (-0.6, 0.4, 0.4, -0.6)$.

3. Bifurcation analysis of the new hyperchaotic system

We now investigate the 4-D system:

$$\dot{y_1} = a(y_2 - y_1) + py_2y_3 = F(y_1, y_2, y_3, y_4), \tag{7a}$$

$$\dot{y_2} = by_2 - y_1y_3 + y_4 = G(y_1, y_2, y_3, y_4), \tag{7b}$$

$$\dot{y_3} = y_1y_2 - cy_3 = H(y_1, y_2, y_3, y_4), \tag{7c}$$

$$\dot{y_4} = -qy_2 = K(y_1, y_2, y_3, y_4), \tag{7d}$$

for arbitrary positive parameter values of a, b, c, p, q. The divergence of the flow is:

$$\frac{\partial F}{\partial y_1} + \frac{\partial G}{\partial y_2} + \frac{\partial H}{\partial y_3} + \frac{\partial K}{\partial y_4} = -(a + c - b). \tag{8}$$

We therefore require $a + c - b > 0$ for contracting flows; the flow is divergence-free if $a + c - b = 0$. For the chosen set of parameter values $(a, b, c) = (40, 28, 3)$, the divergence of the flow equals -15, so volumes contract in phase space.

3.1. Linear stability analysis

The fixed points are found by setting the RHS of (7) to zero. This gives the trivial equilibrium point $(y_1, y_2, y_3, y_4) = (0, 0, 0, 0)$ only. Its linear stability is found by computing the Jacobian matrix, evaluated at the equilibrium value:

$$J = \begin{pmatrix} -a & a & 0 & 0 \\ 0 & b & 0 & 1 \\ 0 & 0 & -c & 0 \\ 0 & -q & 0 & 0 \end{pmatrix}, \tag{9}$$

and then determining the roots of the characteristic equation:

$$(\lambda + c)\lambda^3 + (a - b)\lambda^2 - ab\lambda - q = 0. \tag{10}$$

3.2. Bifurcations

Since $c > 0$, the first eigenvalue is negative, so we focus upon the remaining three eigenvalues. A steady bifurcation, $\lambda = 0$, occurs when $q = 0$. However $q \neq 0$

here, so a steady bifurcation cannot occur. For a Hopf bifurcation, $\lambda = \pm i\omega$, we require

$$\omega^2 = q/(b-a) = ab > 0, \tag{11}$$

so that $b - a > 0$. For the chosen parameter set, this cannot occur, so neither of the two codimension-one bifurcations are possible.

3.3. Nonlinear dynamics

We find it instructive to explore the nonlinear dynamics of the four-dimensional system for parameter values other than the chosen set of values. To do this, we construct bifurcation transition diagrams as each parameter varies in turn, as a function of $x_{\max}$.

Figure 3 shows the bifurcation transition plot of the maxima of $x_{\max}$ as a decreases from $a = 40$. There is a period-four window when $35.85 < a < 36.15$ and another smaller window when $34.75 < a < 35$. The dynamics becomes periodic for $a < 34.35$ and then grows without bound for $a < 29.35$.

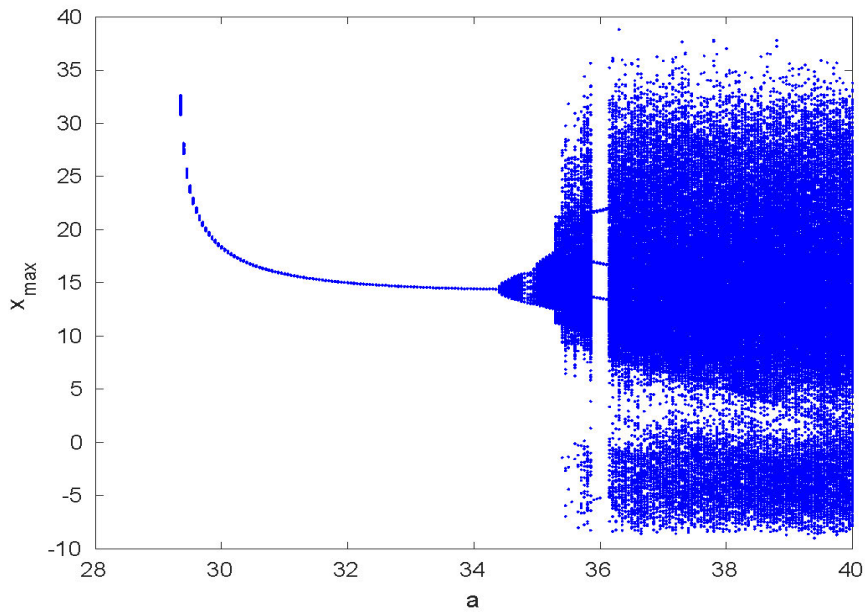

Figure 3: Bifurcation transition plot of $x_{\max}$ as a decreases

Figure 4 shows the corresponding plot when b decreases from $b = 30$. The dynamics is chaotic for $11.7 < b$, before the appearance of a succession of

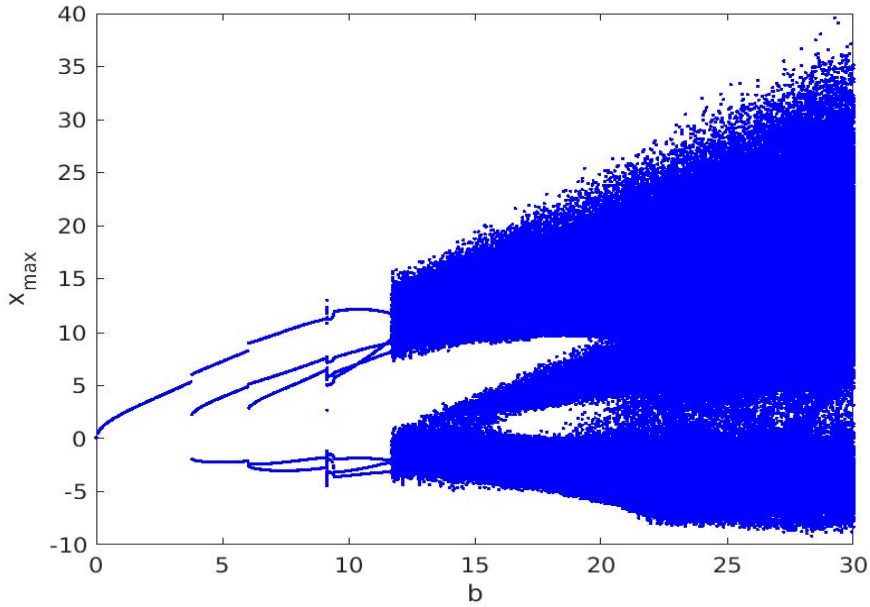

Figure 4: Bifurcation transition plot of $x_{\max}$ as b increases

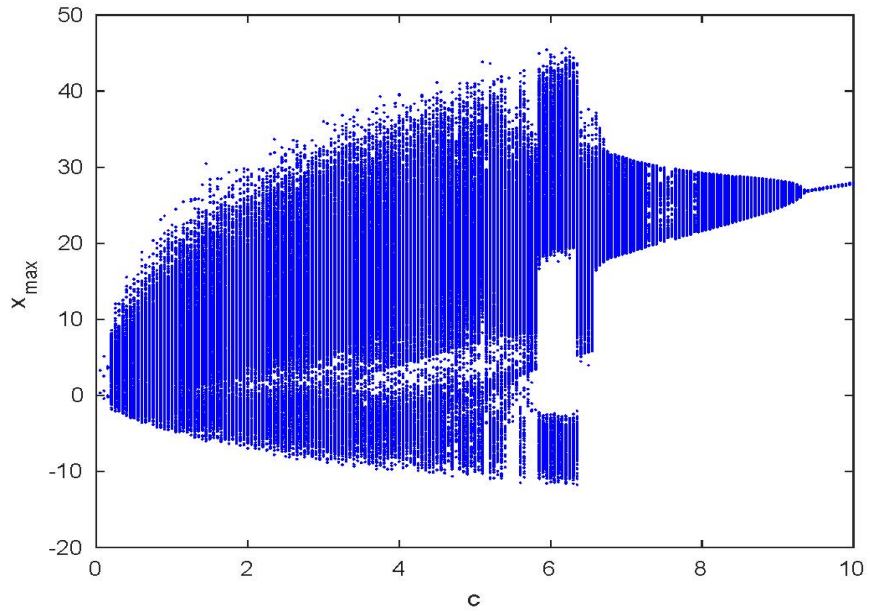

Figure 5: Bifurcation transition plot of $x_{\max}$ as c decreases

periodic branches: period 7 for $9.15 < b < 11.7$; period 5 for $6.05 < b < 9.15$; period 3 for $3.8 < b < 6.05$ and period 1 for $0 < b < 3.8$.

Figure 5 shows the bifurcation transition plot as c decreases from $c = 10$. Here we have periodic states for $9.4 < c$, giving rise to chaotic behaviour between $0.2 < c < 9.4$. There is then a period 4 state for $c = 0.1$ and a period 2 state for $c = 0.05$.

3.4. Dynamics at infinity

3.4.1. Case A

The behaviour of $x_{\max}$ as a decreases, as shown in Figure 3, suggests that we consider the dynamics of Eq. (7) as $x \to \infty$ in order to identify the source of the periodic orbit for $a < 34.35$.

We therefore introduce new variables

$$(y_1, y_2, y_3, y_4) = \left(\frac{1}{X}, \frac{u}{X}, \frac{v}{X}, \frac{w}{X}\right), \qquad t = X\tau. \tag{12}$$

Substitution into Eq. (7) gives $\dfrac{\mathrm{d}}{\mathrm{d}t} \to \dfrac{1}{X}\dfrac{\mathrm{d}}{\mathrm{d}\tau}$ and

$$X_\tau = a(1-u)X^2 - puvX, \tag{13a}$$
$$u_\tau = au(1-u)X - pu^2v + buX - v + wX, \tag{13b}$$
$$v_\tau = av(1-u)X - puv^2 + u - cvX, \tag{13c}$$
$$w_\tau = aw(1-u)X - puvw - quX, \tag{13d}$$

where subscripts denote derivatives with respect to τ.

In order to obtain the dynamics at infinity, we now take the limit $X \to 0$ so that Eq. (13) becomes

$$u_\tau = -v(1 + pu^2), \tag{14a}$$
$$v_\tau = u(1 - pv^2), \tag{14b}$$
$$w_\tau = -puvw, \tag{14c}$$

together with $X_\tau = 0$. From the equations for $u_\tau = 0$ and $v_\tau = 0$, we obtain the fixed point $(u, v) = (0, 0)$. Then $w_\tau = 0$ is automatically satisfied for an arbitrary value for w.

The stability of this fixed point at infinity is found from the eigenvalues of the three-dimensional Jacobian matrix:

$$J_\infty = \begin{pmatrix} -2puv & -1 - pu^2 & 0 \\ 1 & -2puv & 0 \\ -pvw & -puw & -puv \end{pmatrix}, \tag{15}$$

evaluated at $(0, 0, w_{arb})$:

$$J_A = \begin{pmatrix} 0 & -1 & 0 \\ 1 & 0 & 0 \\ 0 & 0 & 0 \end{pmatrix}. \tag{16}$$

The eigenvalues are therefore a pair of pure imaginary eigenvalues $\lambda_{1,2} = \pm i$, and a zero eigenvalue $\lambda_3 = 0$. This is the Jacobian matrix for a codimension-two zero-Hopf bifurcation [23]. The eigenvalues suggest that we have a centre at infinity, and this is the source of the periodic orbits for finite values of the variables y_j, $j = 1, ..., 4$. Moreover, we can find the equation for this periodic orbit at infinity as follows.

From (14c), we get

$$-puv = \frac{w_\tau}{w}. \tag{17}$$

Multiplying (14a) by u, (14b) by v and adding, we get

$$uu_\tau + vv_\tau = -puv\left(u^2 + v^2\right). \tag{18}$$

Substituting from (17) into (18), we get

$$uu_\tau + vv_\tau = \frac{w_\tau}{w}\left(u^2 + v^2\right). \tag{19}$$

We define

$$Y = u^2 + v^2. \tag{20}$$

Then we find that

$$Y_\tau = 2(uu_\tau + vv_\tau) = 2\frac{w_\tau}{w}Y. \tag{21}$$

Separating the variables, we get

$$\frac{Y_\tau}{Y} = 2\frac{w_\tau}{w}. \tag{22}$$

The differential equation (22) can be integrated directly to give

$$u^2 + v^2 = A^2 w^2, \tag{23}$$

for some constant of integration A, which is determined from the initial data for (u, v, w). For example, if we take initial data for our numerical integrations to be $(u, v, w) = (0.5, 0.5, 0.1)$ (the periodic solution, shown in black, in Figure 7), we obtain $A^2 = 50$.

Figure 6 shows the phase portraits of (u, v, w) for the initial data $(1.05, 0.1, 0.1)$: the behaviour is clearly periodic. Figure 7 shows the phase portraits, projected into the (u, v)-plane for 4 choices of initial conditions: $(1.05, 0.1, 0.1)$, $(0.5, 0.1, 0.1)$, $(0.1, 0.1, 0.1)$ and $(0.5, 0.5, 0.1)$. The dynamics is clearly that of a centre at infinity.

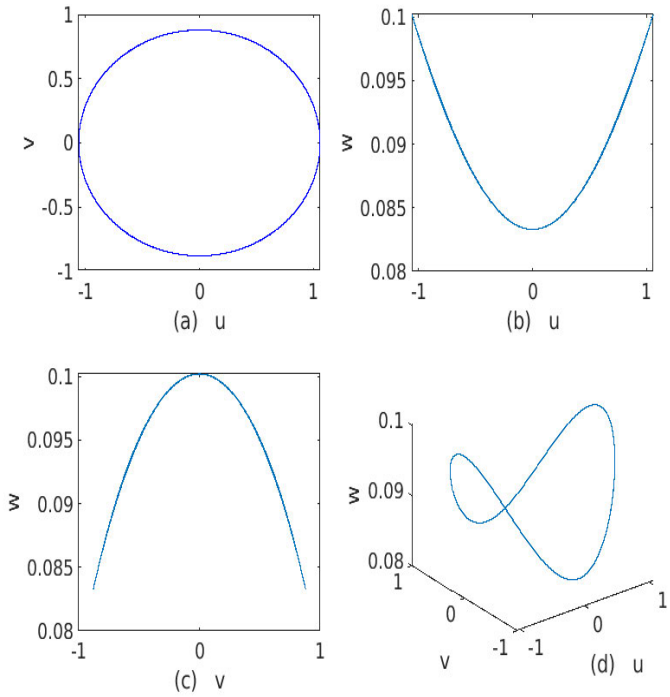

Figure 6: Phase portraits of the equation (14) for the initial data: $(1.05, 0.1, 0.1)$

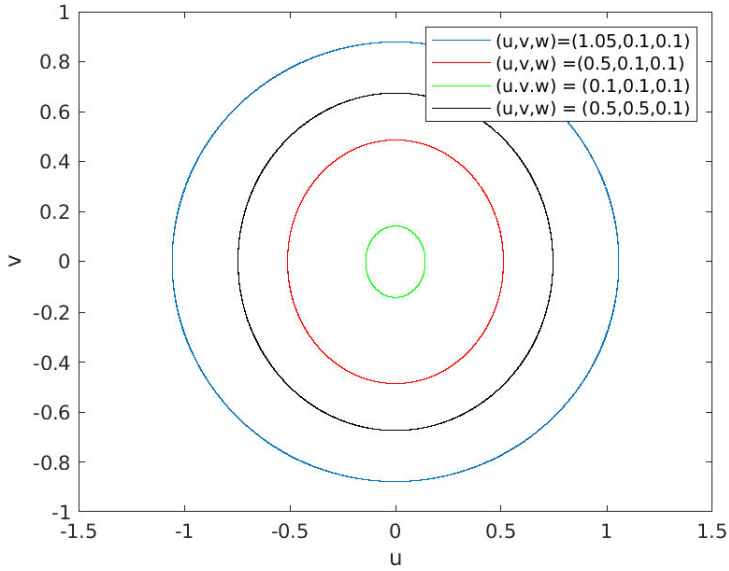

Figure 7: Phase portraits of the equation (14), projected onto the (u, v)-plane for four different initial conditions

3.4.2. Case B

Here, we define

$$(y_1, y_2, y_3, y_4) = \left(\frac{u}{X}, \frac{1}{X}, \frac{v}{X}, \frac{w}{X}\right), \qquad t = X\tau, \tag{24}$$

We substitute into Eq. (7), take the limit $X \to 0$, and obtain

$$u_\tau = v(1 + pu^2), \tag{25a}$$
$$v_\tau = u(1 + v^2), \tag{25b}$$
$$w_\tau = uvw. \tag{25c}$$

We again take the fixed point to be $(u, v, w) = (0, 0, w_{\text{arb}})$, with stability given by the eigenvalues of

$$J_B = \begin{pmatrix} 0 & p & 0 \\ 1 & 0 & 0 \\ 0 & 0 & 0 \end{pmatrix}). \tag{26}$$

This fixed point at infinity is a saddle, with eigenspectrum $\lambda_{1,2} = \pm\sqrt{p}$ and $\lambda_3 = 0$.

3.4.3. Case C

With the change of variables:

$$(y_1, y_2, y_3, y_4) = \left(\frac{u}{X}, \frac{v}{X}, \frac{1}{X}, \frac{w}{X}\right), \qquad t = X\tau, \tag{27}$$

Eq. (7) becomes, as $X \to 0$,

$$u_\tau = v(p - u^2), \tag{28a}$$
$$v_\tau = -u(1 + v^2), \tag{28b}$$
$$w_\tau = -uvw. \tag{28c}$$

Again taking the fixed point as $(u, v, w) = (0, 0, w_{arb})$ as before, the linear stability is found from the eigenspectrum of the Jacobian matrix

$$J_C = \begin{pmatrix} 0 & p & 0 \\ -1 & 0 & 0 \\ 0 & 0 & 0 \end{pmatrix}. \tag{29}$$

We therefore obtain a centre with $\lambda_{1,2} = \pm\sqrt{p}i$ and $\lambda_3 = 0$.

Following the approach used for Case A, we introduce $Y = u^2 + v^2$, and combine Eq. (28) to give

$$\frac{1}{2}Y_\tau = (Y + 1 - p)\frac{w_\tau}{w}, \tag{30}$$

which integrates to give

$$u^2 + v^2 = C^2 w^2 + p - 1, \tag{31}$$

for a constant of integration C.

For the initial condition $(0.5, 0.5, 0.1)$, we obtain $C^2 = 110$. Figure 8 shows the phase portraits of the centre at infinity for initial data of $(0.5, 0.5, 0.1)$.

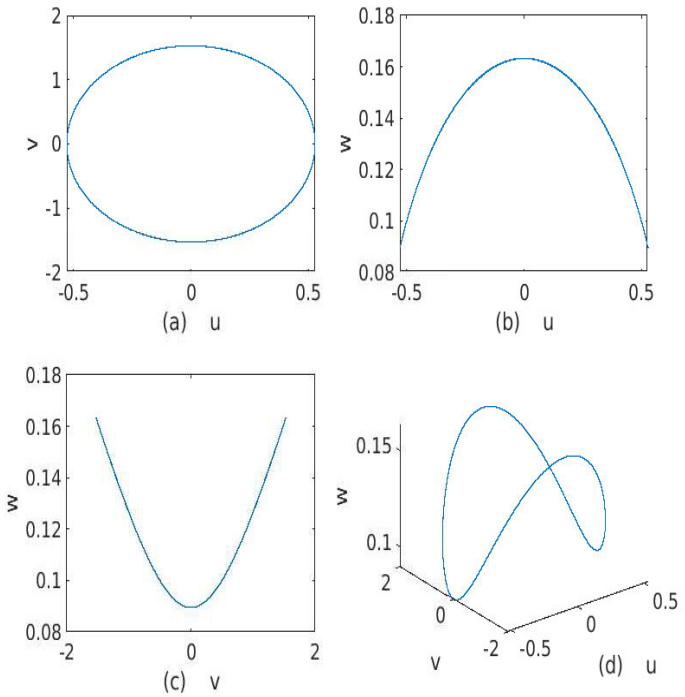

Figure 8: Phase portraits of the equation (28) for the initial data: $(0.5, 0.5, 0.1)$

3.4.4. Case D

Finally the change of variables:

$$(y_1, y_2, y_3, y_4) = \left(\frac{u}{X}, \frac{v}{X}, \frac{w}{X}, \frac{1}{X}\right), \qquad t = X\tau, \tag{32}$$

transforms Eq. (7) to the following:

$$u_\tau = pvw, \tag{33a}$$

$$v_\tau = -uw, \tag{33b}$$

$$w_\tau = uv, \tag{33c}$$

as $X \to 0$.

With $Y = u^2 + v^2$, the system (33) can be combined to give

$$Y_\tau = (p-1)w_\tau^2 \tag{34}$$

with the integral

$$u^2 + v^2 = w^2(p-1) + D, \tag{35}$$

for a constant of integration D.

For the initial condition $(0.5, 0.5, 0.1)$, $D = 0.506$. Because there are no linear terms in Eq. (33), there are three zero eigenvalues for the corresponding Jacobian matrix. Nevertheless, we can integrate system (33) and obtain the periodic phase portraits shown in Figure 9.

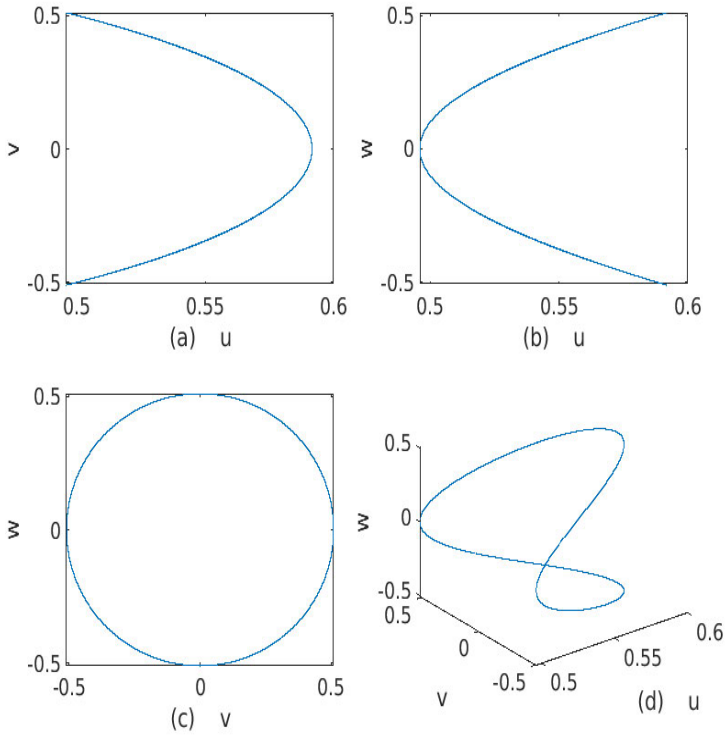

Figure 9: Phase portraits of the equation (33) for the initial data: $(0.5, 0.5, 0.1)$

3.4.5. Summary

In all four systems at infinity, the only parameter which appears (apart from constants of integration, determined from initial data) is the parameter p. In three of the four cases (Cases A, C and D) we observe a stable periodic state, whose equation can be determined exactly by combining the particular system

under consideration. Even for Case B, which yields a saddle point at infinity, we can derive an equation for the orbit. Only the local dynamics depends upon the remaining parameters of the system.

4. Complete synchronization of the new two-scroll hyperchaotic systems

To achieve global synchronization of the new two-scroll hyperchaotic systems, we make use of integral sliding mode control (ISMC), which is a popular technique in the control literature.

The transmitter system is taken as the two-scroll dynamics discussed in Section 2, *viz.*

$$\begin{cases} \dot{y}_1 = a(y_2 - y_1) + py_2y_3\,, \\ \dot{y}_2 = by_2 - y_1y_3 + y_4\,, \\ \dot{y}_3 = y_1y_2 - cy_3\,, \\ \dot{y}_4 = -qy_2\,. \end{cases} \tag{36}$$

We represent $Y = (y_1, y_2, y_3, y_4)$ as the state of the transmitter system (36).

The receiver system is taken as the two-scroll dynamics with controls given by

$$\begin{cases} \dot{w}_1 = a(w_2 - w_1) + pw_2w_3 + V_1\,, \\ \dot{w}_2 = bw_2 - w_1w_3 + w_4 + V_2\,, \\ \dot{w}_3 = w_1w_2 - cw_3 + V_3\,, \\ \dot{w}_4 = -qw_2 + V_4\,. \end{cases} \tag{37}$$

We represent $W = (w_1, w_2, w_3, w_4)$ as the state of the receiver system (37).

We denote $V = (V_1, V_2, V_3, V_4)$ as the sliding mode controller which is to be designed in this section so as to completely synchronize the respective states of the transmitter system (36) and the receiver system (37).

The synchronization error for the transmitter system (36) and the receiver system (37) is described as follows:

$$\begin{cases} \chi_1 = w_1 - y_1\,, \\ \chi_2 = w_2 - y_2\,, \\ \chi_3 = w_3 - y_3\,, \\ \chi_4 = w_4 - y_4\,. \end{cases} \tag{38}$$

It is easy to see that

$$\begin{cases} \dot{\chi}_1 = a(\chi_2 - \chi_1) + p(w_2w_3 - y_2y_3) + V_1\,, \\ \dot{\chi}_2 = b\chi_2 + \chi_4 - w_1w_3 + y_1y_3 + V_2\,, \\ \dot{\chi}_3 = -c\chi_3 + w_1w_2 - y_1y_2 + V_3\,, \\ \dot{\chi}_4 = -q\chi_2 + V_4\,. \end{cases} \tag{39}$$

In the IMSC design, we associate an integral sliding surface with every synchronization error variable χ_i, $(i = 1, 2, 3, 4)$ as follows:

$$\begin{cases} S_1 = \chi_1 + \mu_1 \displaystyle\int_0^t \chi_1(\alpha)\,\mathrm{d}\alpha\,, \\ S_2 = \chi_2 + \mu_2 \displaystyle\int_0^t \chi_2(\alpha)\,\mathrm{d}\alpha\,, \\ S_3 = \chi_3 + \mu_3 \displaystyle\int_0^t \chi_3(\alpha)\,\mathrm{d}\alpha\,, \\ S_4 = \chi_4 + \mu_4 \displaystyle\int_0^t \chi_4(\alpha)\,\mathrm{d}\alpha\,. \end{cases} \tag{40}$$

Differentiating the equations given in (40), we obtain:

$$\begin{cases} \dot{S}_1 = \dot{\chi}_1 + \mu_1 \chi_1\,, \\ \dot{S}_2 = \dot{\chi}_2 + \mu_2 \chi_2\,, \\ \dot{S}_3 = \dot{\chi}_3 + \mu_3 \chi_3\,, \\ \dot{S}_4 = \dot{\chi}_4 + \mu_4 \chi_4\,. \end{cases} \tag{41}$$

We suppose that μ_1, μ_2, μ_3 and μ_4 are positive constants, and consider the integral sliding mode controls as follows:

$$\begin{aligned} V_1 &= -a(\chi_2 - \chi_1) - p(w_2 w_3 - y_2 y_3) - \mu_1 \chi_1 - \epsilon_1 \mathrm{sgn}(S_1) - \kappa_1 S_1\,, \\ V_2 &= -b\chi_2 - \chi_4 + w_1 w_3 - y_1 y_3 - \mu_2 \chi_2 - \epsilon_2 \mathrm{sgn}(S_2) - \kappa_2 S_2\,, \\ V_3 &= c\chi_3 - w_1 w_2 + y_1 y_2 - \mu_3 \chi_3 - \epsilon_3 \mathrm{sgn}(S_3) - \kappa_3 S_3\,, \\ V_4 &= q\chi_2 - \mu_4 \chi_4 - \epsilon_4 \mathrm{sgn}(S_4) - \kappa_4 S_4\,. \end{aligned} \tag{42}$$

In Eq. (42), μ_i, τ_i, κ_i, $(i = 1, 2, 3, 4)$ are positive constants.
Substituting (42) into the error dynamics (39), we obtain the following:

$$\begin{cases} \dot{\chi}_1 = -\mu_1 \chi_1 - \epsilon_1\, \mathrm{sgn}(S_1) - \kappa_1 S_1\,, \\ \dot{\chi}_2 = -\mu_2 \chi_2 - \epsilon_2\, \mathrm{sgn}(S_2) - \kappa_2 S_2\,, \\ \dot{\chi}_3 = -\mu_3 \chi_3 - \epsilon_3\, \mathrm{sgn}(S_3) - \kappa_3 S_3\,, \\ \dot{\chi}_4 = -\mu_4 \chi_4 - \epsilon_4\, \mathrm{sgn}(S_4) - \kappa_4 S_4\,. \end{cases} \tag{43}$$

The following theorem states the main control result for this system on the synchronization of the two-scroll hyperchaotic systems (36) and (37).

Theorem 1 *The integral sliding mode control law (42) renders the transmitter system (36) and receiver system (37) synchronized globally for all values of initial states* $Y(0)$, $W(0)$ *in* $\mathbb{R}^4$, *where it is assumed that* $\mu_i, \epsilon_i, \kappa_i, (i = 1, 2, 3, 4)$ *are positive constants.*

Proof. We start the proof by taking the Lyapunov function defined by

$$V(S_1, S_2, S_3, S_4) = \frac{1}{2}\left(S_1^2 + S_2^2 + S_3^2 + S_4^2\right). \tag{44}$$

We note that V takes all non-negative values. Also, $V = 0$ if and only if $S_1 = S_2 = S_3 = S_4 = 0$.

This shows that V is a quadratic and strictly positive definite function on $\mathbb{R}^4$.

Next, we find that

$$\dot{V} = S_1\dot{S}_1 + S_2\dot{S}_2 + S_3\dot{S}_3 + S_4\dot{S}_4\,. \tag{45}$$

A simple calculation shows that

$$\dot{V} = \sum_{i=1}^{4} S_i\big(-\epsilon_i\,\mathrm{sgn}(S_i) - \kappa_i S_i\big) \tag{46}$$

which can be simplified as follows:

$$\dot{V} = -\sum_{i=1}^{4}\left[\epsilon_i|S_i| + \kappa_i S_i^2\right]. \tag{47}$$

Since $\epsilon_i > 0$ and $\kappa_i > 0$ for $i = 1, 2, 3, 4$, $\dot{V}$ is a negative definite function defined on $\mathbb{R}^4$.

Using Lyapunov stability theory, it is deduced that $S_i(t) \to 0$, $(i = 1, 2, 3, 4)$ as $t \to \infty$.

Hence, it follows that $\chi_i(t) \to 0$, $(i = 1, 2, 3, 4)$ as $t \to \infty$.

This completes the proof. □

For MATLAB simulations, the constants are considered as in the hyperchaos case, *viz.* $(a, b, c, p, q) = (40, 28, 3, 0.4, 2.5)$.

Let us assume the sliding constants as $\epsilon_i = 0.3$, $\kappa_i = 12$ and $\mu_i = 12$ for $i = 1, 2, 3, 4$.

The initial state of the transmitter system (36) is taken as

$$y_1(0) = 4.2, \quad y_2(0) = 8.3, \quad y_3(0) = 7.2, \quad y_4(0) = 1.6. \tag{48}$$

The initial state of the receiver system (37) is taken as

$$w_1(0) = 3.8, \quad w_2(0) = 5.4, \quad w_3(0) = 12.6, \quad w_4(0) = 15.9. \tag{49}$$

The sliding controller design based on the 4-D hyperchaotic systems (36) and (37) is illustrated in the Figure 10.

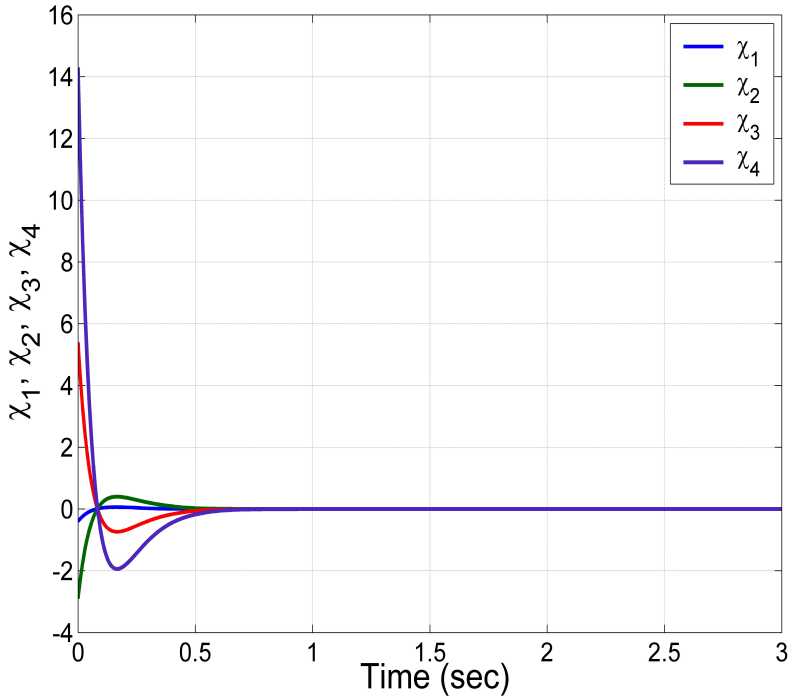

Figure 10: MATLAB plot showing complete synchronization errors with time-history for the 4-D hyperchaotic systems (36) and (37)

5. Circuit simulation of the new 4D Hyperchaotic System

In this work, the new 4D hyperchaotic system is realized by the NI MultiSIM 14.0 platform. The electronic circuit design of the proposed hyperchaotic system is shown in Figure 11.

Applying the Kirchhoff laws, the circuit presented in Figure 11 is described by the following equations:

$$\begin{cases} \dot{y_1} = \dfrac{1}{C_1R_1}y_2 - \dfrac{1}{C_1R_2}y_1 + \dfrac{1}{10C_1R_3}y_2y_3\,, \\ \dot{y_2} = \dfrac{1}{C_2R_4}y_2 - \dfrac{1}{10C_2R_5}y_1y_3 + \dfrac{1}{C_2R_6}y_4\,, \\ \dot{y_3} = \dfrac{1}{10C_3R_7}y_1y_2 - \dfrac{1}{10C_3R_8}y_3 \\ \dot{y_4} = -\dfrac{1}{C_4R_9}y_2\,. \end{cases} \tag{50}$$

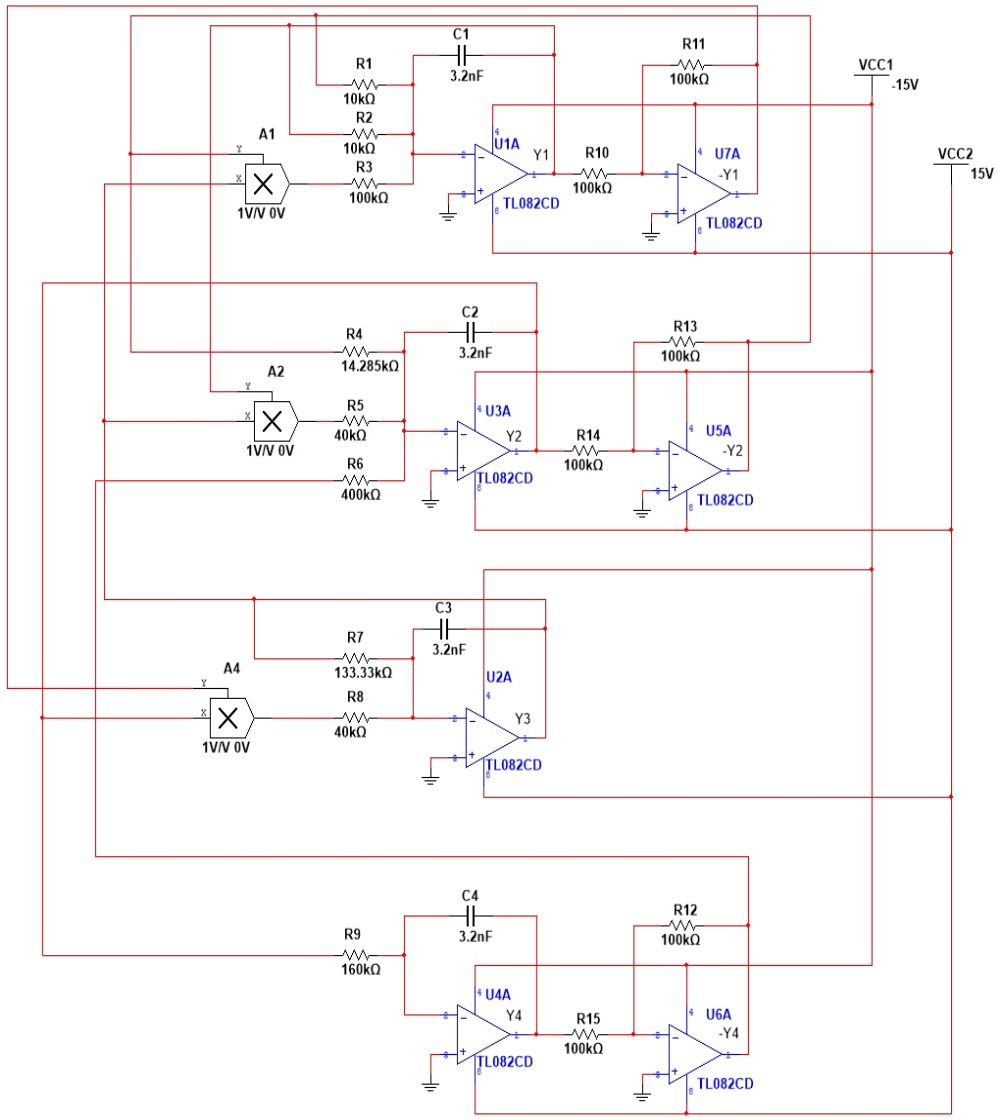

Figure 11: Circuit design of the new two-scroll hyperchaotic system

Here, y_1, y_2, y_3, y_4 correspond to the voltages on the integrators U1A, U2A, U3A and U4A, respectively. The values of components in the circuit are selected as: $R_1 = R_2 = 10$ kΩ, $R_4 = 14.285$ kΩ, $R_5 = R_8 = 40$ kΩ, $R_6 = 400$ kΩ, $R_7 = 133.33$ kΩ, $R_9 = 160$ kΩ, $R_3 = R_{10} = R_{11} = R_{12} = R_{13} = R_{14} = R_{15} = 100$ kΩ, $C_1 = C_2 = C_3 = C_4 = 3.2$ nF. MultiSIM outputs of the circuit are presented in Figure 12. These results are consistent with the numerical simulation results presented in Section 2.

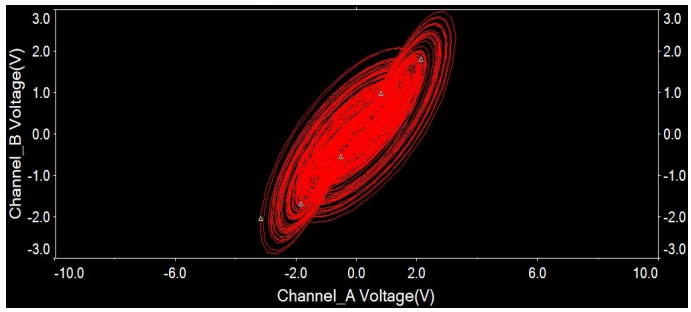

(a)

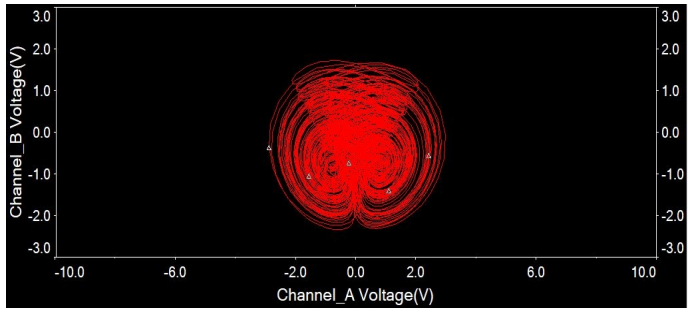

(b)

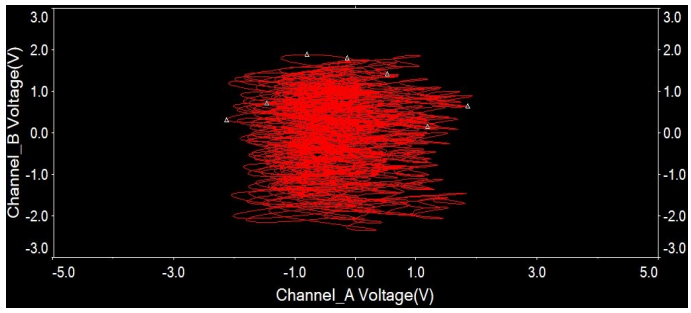

(c)

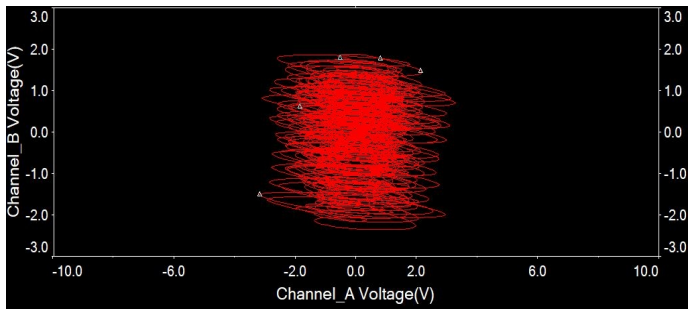

(d)

Figure 12: Hyperchaotic attractors of new 4D Hyperchaotic system using NI MultiSIM circuit simulation: (a) y_1-y_2 plane, (b) y_2-y_3 plane, (c) y_3-y_4 plane and y_1-y_4 plane

6. Conclusions

A two-scroll 4-D hyperchaotic system with a unique saddle point equilibrium at the origin was proposed in this work and the bifurcation properties of the new system were discussed in detail. Using integral sliding mode control (ISMC), we designed a nonlinear control for the complete synchronization of a pair of two-scroll hyperchaotic systems developed in this work. Finally, as an electronic application, we simulated the new 4-D two-scroll hyperchaotic system using Multisim for real-world implementations.

References

[1] Y.J. Monkam, S.T. Kingni, R. Tchitnga and P. Woafo: Electronic simulation and microcontroller real implementation of an autonomous chaotic and hyperchaotic system made of a Colpitts-Josephson junction like circuit. *Analog Integrated Circuits and Signal Processing*, **110**(3), (2022), 395–407. DOI: 10.1007/s10470-021-01965-1.

[2] J. Petrzela: Chaotic and hyperchaotic self-oscillations of lambda diode composed by generalized bipolar transistors. *Applied Sciences,* **11**(8), (2021), Article ID 3326. DOI: 10.3390/app11083326.

[3] J.P. Singh, K. Rajagopal and B.K. Roy: Switching between dissipative and conservative behaviors in a modified hyperchaotic system with the variation of its parameter. *International Journal of Bifurcation and Chaos*, **31**(16) (2021), Article ID 2130048-8. DOI: 10.1142/S0218127421300482.

[4] Y. Jiang, C. Li, C. Zhang, Y. Zhao and H. Zang: A double-memristor hyperchaotic oscillator with complete amplitude control. *IEEE Transactions on Circuits and Systems I: Regular Papers,* **68**(12), (2021), 4935–4944. DOI: 10.1109/TCSI.2021.3121499.

[5] D. Yan, L. Wang, S. Duan and J. Chen: Designing twin memristor-based multiscroll systems by varying the flux variable of memristor. *International Journal of Bifurcation and Chaos,* **31**(7), (2021), Article ID 2150099. DOI: 10.1142/S0218127421500991.

[6] R. Li and R. Ding: A simple time-delay memristor and its application in 2D HR neuron model. *International Journal of Modern Physics B,* **35**(13), (2021), Article ID 2150166. DOI: 10.1142/S0217979221501666.

[7] S. Yan, E. Wang, Q. Wang, X. Sun and Y. Ren: Analysis, circuit implementation and synchronization control of a hyperchaotic system. *Physica Scripta,* **96**(12), (2021), Article ID 125257. DOI: 10.1088/1402-4896/ac379b.

[8] S. Vaidyanathan, S. He and A. Sambas: A new multistable double-scroll 4-D hyperchaotic system with no equilibrium point, its bifurcation analysis, synchronization and circuit design. *Archives of Control Sciences,* **31**(1), (2021), 99–128. DOI: 10.24425/acs.2021.136882.

[9] S. Vaidyanathan, I.M. Moroz and A. Sambas: A new 4-D hyperchaotic system with no equilibrium, its multistability, offset boosting and circuit simulation. *Archives of Control Sciences,* **30**(3), (2020), 575–597. DOI: 10.24425/acs.2020.134678.

[10] X. Wang, M. Gao, X. Min, Z. Lin and H. Ho-Ching Iu: On the use of memristive hyperchaotic system to design color image encryption scheme. *IEEE Access,* **8** (2020), 182240–182248. DOI: 10.1109/ACCESS.2020.3027480.

[11] G.D. Leutcho, H. Wang, T.F. Fozin, K. Sun, Z.T. Njitacke and J. Kengne: Dynamics of a new multistable 4D hyperchaotic Lorenz system and its applications. *International Journal of Bifurcation and Chaos,* **32**(1), (2022), Article ID 2250001. DOI: 10.1142/S0218127422500018.

[12] B. Ge, X. Chen, G. Chen and Z. Shen: Secure and fast image encryption algorithm using hyper-chaos-based key generator and vector operation. *IEEE Access,* **9** (2021), 137635–137654. DOI: 10.1109/ACCESS.2021.3118377.

[13] M. Liu, M. Yu, J. Wang, Y. Chen and Y. Bian: Design of 9-D global chaotic system and its application in secure communication. *Circuit World*, **48**(1), (2022), 88–104. DOI: 10.1108/CW-03-2020-0042.

[14] S. Vaidyanathan, A. Sambas, E. Tlelo-Cuautle, A.A. Abd El-Latif, B. Abd-El-Atty, O. Giullen-Fernandez, K. Benkouider, M.A. Mohamed, M. Mamat and M.A.H. Ibrahim: A new 4-D multi-stable hyperchaotic system with no balance point: Bifurcation analysis, circuit simulation, FPGA realization and image cryptosystem. *IEEE Access*, **9** (2021), 144555–144573. DOI: 10.1109/ACCESS.2021.3121428.

[15] K. Behih, S.E. Saadi and Z. Bouchama: Hyperchaos synchronization using T-S fuzzy model based synergetic control theory. *International Journal of Intelligent Engineering and Systems*, **14**(6), (2021), 588–595. DOI: 10.22266/ijies2021.1231.52.

[16] T.L. Le: Multilayer interval type-2 fuzzy controller design for hyperchaotic synchronization. *IEEE Access*, **9** (2021), 155286–155296. DOI: 10.1109/access.2021.3126880.

[17] X. Li, C. Zheng, X. Wang, Y. Cao and G. Xu: Symmetric coexisting attractors and extreme multistability in chaotic system. *Modern Physics Letters B*, **35**(32), (2021), Article ID 2150458. DOI: 10.1142/S0217984921504583.

[18] J. Shi, K. He and H. Fang: Chaos, Hopf bifurcation and control of a fractional-order delay financial system. *Mathematics and Computers in Simulation*, **194** (2022), 348–364. DOI: 10.1016/j.matcom.2021.12.009.

[19] G.D. Leutcho, H. Wang, T.F. Fozin, K. Sun Z.T. Njitacke and J. Kengne: Dynamics of a new multistable 4D hyperchaotic Lorenz system and its applications. *International Journal of Bifurcation and Chaos*, **32**(1), (2022), Article ID 2250001. DOI: 10.1142/S0218127422500018.

[20] N. Mazhar, F.M. Malik, A. Raza and R. Khan: Predefined-time control of nonlinear systems: A sigmoid function based sliding manifold design approach. *Alexandria Engineering Journal*, **61**(9), (2022), 6831–6841. DOI: 10.1016/j.aej.2021.12.030.

[21] A.R. Periyanagayam and Y.H. Joo: Integral sliding mode control for increasing maximum power extraction efficiency of variable-speed wind energy system. *International Journal of Electrical Power and Energy Systems*, **139** (2022), Article ID 107958. DOI: 10.1016/j.ijepes.2022.107958.

[22] J. Ansari, A. Reza Abbasi and B. Bahmani Firouzi: Decentralized LMI-based event-triggered integral sliding mode LFC of power systems with disturbance observer. Integral sliding mode control for increasing maximum power extraction efficiency of variable-speed wind energy system. *International Journal of Electrical Power and Energy Systems*, **138** (2022), Article ID 107971. DOI: 10.1016/j.ijepes.2022.107971.

[23] J. Guckenheimer and P. Holmes: *Nonlinear Oscillations, Dynamical Systems, and Bifurcations of Vector Fields.* Springer, New York, NY, USA, 1983.